Desalination and Water Treatment
www.deswater.com
doi: 10.1080/19443994.2016.1140083

57 (2016) 24176–24186
November

Taylor & Francis
Taylor & Francis Group

Using the Spiegler–Kedem model to predict solute rejection in the treatment of industrial UHT condensates by reverse osmosis

Adrián Suárez, Francisco A. Riera*

Department of Chemical and Environmental Engineering, University of Oviedo, Julián Clavería 8, Oviedo 33006, Spain, Tel. +34 985103436; Fax: +34 985103434; emails: a.s.g_86@hotmail.com (A. Suárez), far@uniovi.es (F.A. Riera)

Received 12 September 2015; Accepted 5 January 2016

ABSTRACT

Flash cooler condensates from the ultra-high-temperature process of a commercial dairy were treated *in situ* by reverse osmosis at a semi-industrial scale with the objective of modelling the membrane rejection. These multi-component streams, unlike the synthetic solutions used in theoretical studies, proved to be strongly heterogeneous. Their inorganic and organic loads were measured in terms of conductivity and chemical oxygen demand, respectively, and membrane rejection for these parameters was evaluated at different permeate fluxes (between 55 and 105 L/hm^2, approximately) and concentrations (between 197.5 and 1143.0 μS/cm conductivity and 67 and 289 mgO_2/L chemical oxygen demand). The Spiegler–Kedem and combined–film theory–Spiegler–Kedem models were brought face to face and their precision was checked. Although no significant differences were found when modelling conductivity rejection, the latter model produced the lowest relative error (1.82%) when comparing the observed and estimated rejections of organic matter, which provided evidence of the advantages of considering the concentration polarisation phenomenon.

Keywords: Modelling; Concentration polarisation; Reverse osmosis; Commercial dairy; Wastewater reclamation

1. Introduction

Predicting the performance of high-pressure membrane applications leads to process optimisation [1]. Several review works can be found in the literature regarding nanofiltration (NF) and reverse osmosis (RO) modelling by mechanistic or mathematical development [2,3]. The models are generally classified into those based on transport mechanisms/hydrodynamics (solution–diffusion, Kimura–Sourirajan, extended Nerst–Plank models, etc.) and those derived from the irreversible thermodynamics (Kedem–Katchalsky, Spiegler–Kedem (SK) models, etc.) [4,5]. Although most of them are strongly related, some models show complex mathematic equations and require sophisticated solution techniques [6]. Furthermore, the information which must be entered for the model, such as the pore geometry, solute diffusion coefficients, etc., is frequently unknown and its determination complex and impractical for use in industrial conditions [7].

In order to describe the performance of RO, the phenomenological SK model [8] has been extensively recommended and used [9–12]. It is based on the consideration that the solvent and solute fluxes are both

*Corresponding author.

dependent on the differences in chemical potential, caused either by concentration or pressure gradients (driving forces) between the sides of the membrane [4]. The membrane is considered a black box by neglecting its porosity and where no specific knowledge of transport mechanisms and membrane structure is required [13], making the methodology more accessible but providing no insight into the mechanism of separation [14]. Additionally, the electrostatic potential of the system is not taken into account as the model assumes the membrane to be uncharged [15]. Not only has the SK model been used to predict salt [16] and organic compound [17] transport across the membrane in single and binary solute systems, but it has also been applied in the field of multi-component separation description, and for this reason, it is very useful in RO industrial processes [4].

The SK model defines the membrane transport as a combination of convection, resulting from the applied transmembrane pressure (ΔP), and diffusion, a consequence of the concentration gradient (dC/dx) [18]. It is a two-parameter model described by the solute permeability (P_s) and the reflection coefficient (σ), both obtained by a fitting procedure in rejection trials [19]. The relevant equation for the SK model (Eq. (1)) defines the solute flux (J_s) across the membrane as follows:

$$J_S = P_S \Delta x \frac{dC}{dx} + (1-\sigma) J_V C \tag{1}$$

where C represents the solute concentration and J_v the permeate flux, which is defined by the following Eq. (2) [20]:

$$J_V = L_p(\Delta P - \sigma\pi) \tag{2}$$

The L_p being the membrane permeability and $\Delta\pi$, the osmotic pressure. Integrating Eq. (1) over the membrane thickness (Δx) and introducing the rejection definition (supposing the concentration at the membrane surface (C_m), difficult to obtain experimentally, equal to that of the feed (C_f)), an expression (Eq. (3)) to relate the estimated rejection (R_{est}; expressed in %) and J_v is obtained [21]:

$$R_{est} = \left(1 - \frac{1-\sigma}{1-\sigma e^{-\frac{(1-\sigma)Jv}{P_s}}}\right) \times 100 \tag{3}$$

where P_s is a measure of the diffusive transport, while σ, which influences the convective term, is the maximum rejection possible for a given component, and corresponds with the rejection at the idealised condition of infinite solvent flux [22].

One of the main drawbacks when applying the standard SK model is that there is no consideration of the concentration polarisation (CP) effect, so a correction of the model should be provided as this phenomenon is one of the most important factors influencing the membrane design process [23]. CP, which is considered a reversible effect, occurs within a boundary film facing the membrane/feed solution interface when an increase in the local concentration is created by the retained species which accumulate at the membrane surface [24]. This effect causes an increase in the osmotic pressure and, consequently, a reduction in the net driving forces of the system [25]. Neglecting this phenomenon may result in inaccurate determinations of L_p and σ, and could lead to overestimation of water quality and recovery in case of wastewater reclamation applications [26].

In order to take into account the CP effect, the SK model has been coupled to the film theory (resulting in the combined–film theory–Spiegler–Kedem or CFSK model [14]), which assumes that, at steady state, the thickness of the polarisation layer (δ) is established at the equilibrium of the convective fluxes towards and through the membrane and the back diffusive flux. The mass balance generated is solved within the boundary conditions by Eq. (4), which could be combined with the SK model to obtain a relationship between R_{est} (expressed in %) and J_v (Eq. (5)) [21].

$$\frac{Cm - Cp}{C_f - C_p} = e^{\frac{\delta}{D}Jv} \tag{4}$$

$$R_{est} = \left(1 - \frac{1}{1 + \frac{\sigma}{1-\sigma}\left[e^{-\frac{\delta}{D}Jv} - e^{-\frac{(1-\sigma)Jv}{P_s}\frac{\delta}{D}Jv}\right]}\right) \times 100 \tag{5}$$

The permeate concentration and the solute diffusivity are C_p and D, respectively. The D/δ ratio corresponds with the mass transfer coefficient (k). At any rate, k could be simultaneously calculated (and specifically for the membrane configuration selected) with P_s and σ through experimental data of observed rejection (R_{obs}) and J_v by a fitting procedure as well. The major deficiencies found when applying this model are the assumption that k is constant, when it is often concentration dependent, and the consideration of concentration linearity in the boundary layer [27].

The mathematical models previously described have been frequently tested with synthetic solutions; however, their usefulness has not been studied in depth in the case of industrial processes where feed composition and heterogeneity introduce extra

difficulty in the prediction of fluxes and rejections [28]. Some previous works published by the authors [29–31] have demonstrated the possibility of reusing low-polluted flash cooler (FC) condensates, from the direct ultra-high-temperature (UHT) process of a commercial dairy, with the purpose of boiler water production by RO. In this technical paper, the SK and CFSK models have been tested to this application at a semi-industrial scale, and the model parameters estimated experimentally. Due to the complexity of the composition of these condensates, membrane selectivity of salts and organic matter has been measured indirectly in terms of conductivity and chemical oxygen demand (COD), respectively.

Table 1
Duratherm® HWS 4040 HR membrane characteristics

Material: proprietary composite (TFC membrane)	
Average salt rejection[a], %	99.5
Maximum crossflow, m^3/h	4.5
Spacer thickness, mil	31
Active area, m^2	8.2
Maximum operating pressure, bar	
5–50°C	41.4
51–70°C	20.7
Maximum operating temperature, °C	70
pH operating range	4.0–11.0

[a]Testing conditions: 2,000 mg/L NaCl solution at 15.5 bar operating pressure, 25ºC, pH 7.5 and 15% recovery before any hot-water sanitisation.

2. Materials and methods

2.1. Reverse osmosis pilot plant

Two spiral-wound thin-film composite (TFC) Duratherm® HWS 4040 HR membranes (GE Water & Process Technologies, USA) were installed in series as part of the RO rig described in Fig. 1, the properties of this specific RO membrane being given in Table 1. The RO plant was fed with condensates from one of the four FCs operating in a Spanish commercial dairy, the RO trials being performed *in situ*. The established membrane cleaning protocol was a sequence of acid (20 min, 45°C) and alkali (45 min, 45°C) steps with Divos 2 and Divos 123 (Diversey, The Netherlands), respectively. Cleaning was carried out between each set of experiments, the reference permeability being fully recovered in all cases. On the other hand, and in order to maintain low values of water silt density index (SDI) for rinsing and cleaning purposes, a prefiltration system, consisting of a bag filter (BF-01) and three cartridge prefilters *F*-01, *F*-02 and *F*-03 of 5, 1 and 0.2 μm, respectively, was installed.

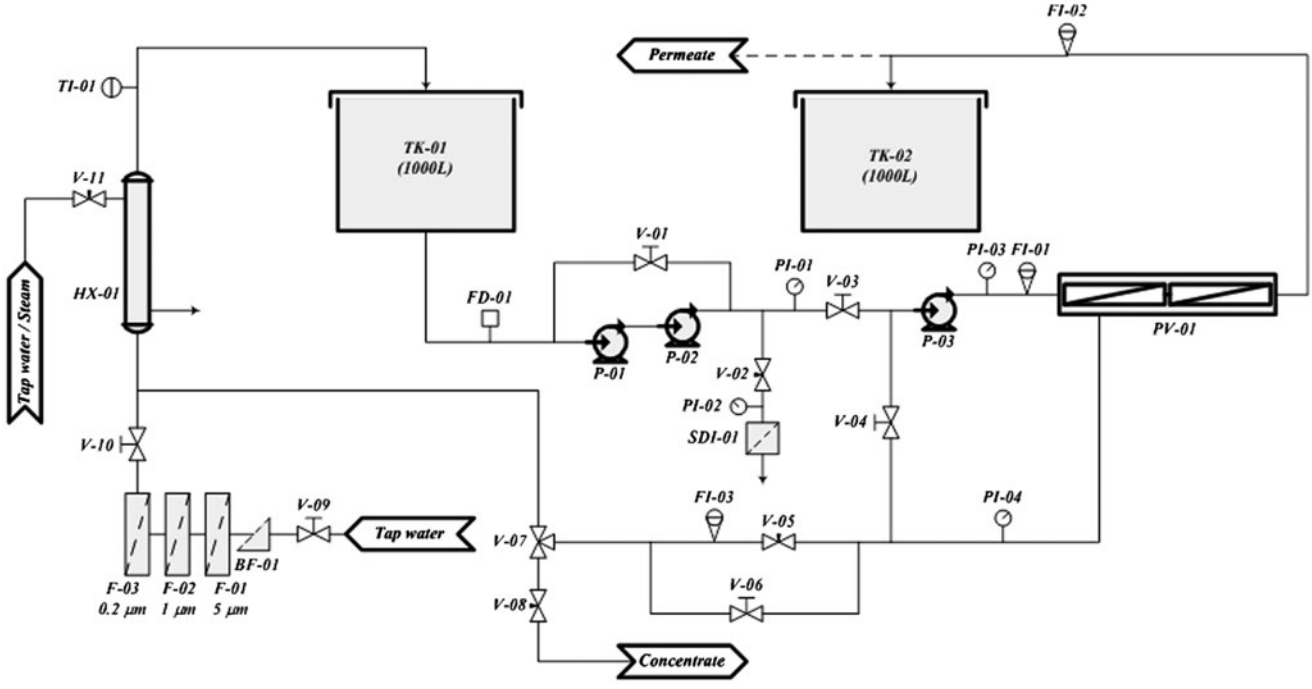

Fig. 1. Scheme of the RO pilot plant.

The FC condensates were collected in a 1,000-L feed tank (TK-01) and fed to the RO pressure vessel (PV-01) through a set of high pressure pumps (*P*-01 and *P*-02 (Lowara, Italy); 2.2 and 3.0 kW, respectively). A flow detector (FD-01) was installed before the pumps to avoid the system working under vacuum. The ΔP was controlled by regulating the needle valve (*V*-05) located on the concentrate line and monitored by the pressure indicators (PI) of the system. The flow in the feed, concentrate and permeate channels was measured by their respective flow meters (FI), and the temperature controlled and adjusted by a temperature indicator (TI-01) and a heat exchanger (HX-01), respectively.

2.2. Operating procedure and conditions

The trials were performed discontinuously through a semi-closed loop where the permeate produced in the RO pilot plant was stored in an external 1,000-L tank (TK-02, Fig. 1) and the concentrate returned to the feed tank. In this way, a certain degree of concentration was achieved as the system worked at increasing values of the volume concentration ratio (VCR), a parameter defined by Eq. (6).

$$\mathrm{VCR} = \frac{V_f}{V_c} = \frac{V_f}{V_f - V_p} \tag{6}$$

where V_f, V_c and V_p are the feed, concentrate and permeate volumes, respectively.

The feed flow rate and temperature were fixed at approximately 2.5 m^3/h and 52.5 ± 1.5°C, respectively, and the different tests were performed at variable VCRs (1–10) and ΔPs (10–20 bar). The J_v was continuously measured and the R_{obs} for the main parameters, i.e. COD and conductivity, studied, determined at different operating conditions by means of the Eq. (7).

$$R_{obs} = \left(1 - \frac{Cp}{C_f}\right) \times 100 \tag{7}$$

where C_p and C_f are the permeate and feed concentration values of both parameters considered, respectively.

2.3. Analytical methods

The fresh FC condensates and resultant RO permeates were characterised in terms of pH (accuracy ±0.05), electrical conductivity (accuracy ±0.5%) and COD (accuracy ±3 mgO_2/L). A more complete analysis of these streams was previously published by Riera et al. [32] and Suárez and Riera [31]. pH, corrected with temperature, and electrical conductivity, referenced at 25°C, were measured by an HQ40d multimeter (Hach Lange, Belgium). COD was determined spectrophotometrically by previous Cr^{3+} determination at 605 nm using a Spectroquant NOVA 60 photometer (Merck, Germany) after a sulphuric oxidation in a cell test.

2.4. Determination of model parameters

The two parameters P_s and σ of the SK model, and the three parameters of the CFSK model (P_s, σ and k) were estimated by a non-linear fitting procedure linked to a least-squares algorithm (*Solver* tool, Microsoft Excel) of the pairs of values (J_v, R_{obs}) obtained for each concentration (VCR). So, these experimental data were fitted to Eq. (3) when considering the SK model and Eq. (5) regarding the CFSK model, the respective model parameters being those that minimised the squared differences between the observed and predicted rejections, $(R_{obs}–R_{est})^2$.

3. Results and discussion

Discontinuous testing allowed to obtain the pairs of values (J_v, R_{obs}) required to test the mathematical models at different feed concentrations. The heterogeneity of the real industrial water hindered the repeatability of the initial starting conditions and, as a result, the feed composition of the different trials showed certain variability (pH: 6.02 ± 0.15; conductivity: 197.5 ± 10.6 μS/cm; COD: 67 ± 10 mgO_2/L; at VCR 1). The standard deviation gained importance, in general, with growing concentration (pH: 7.27 ± 0.07; conductivity: 1143.0 ± 79.0 μS/cm; COD: 289 ± 76 mgO_2/L; at VCR 10).

The permeability of the membrane with prefiltered tap water (SDI < 3) at 50°C was previously measured giving a value of 6.9 L/hm^2 bar [31]. When processing condensates in a batch, the permeate flux showed a linear dependency with ΔP up to 15 bar, the flux percentage improvement being almost constant (33.3 ± 2.4%) in all cases when increasing the pressure from 10 to 15 bar at the different VCRs studied. However, this linearity was lost at higher pressures, as observed by Turan [33] too, as the flux increment when changing from 15 to 20 bar was only maintained at VCR 1 (29.8%). Moreover, this flux increment was reduced when increasing the concentration of the feed solution (20.2, 17.5, 16.0 and 14.9% at VCR 2, 3.3, 5 and 10, respectively). Higher salt concentration increases the

osmotic pressure, thus reducing the driving pressure and therefore the permeate flux [13], although at the low concentrations used in this work, the osmotic contribution can be neglected. The decreasing slope of the curve J_v vs. ΔP at certain pressures could be associated with the occurrence of CP phenomena [34], the resistance to permeation being higher with the increased concentration of solutes at the surface of the membrane [24]. Other authors associate it to membrane compaction at high working pressures [35].

The experimental R_{obs} at each J_v was used to determine the parameters P_s, σ (expressed in %) and k of the SK and the CFSK models, the main results being collected in Table 2. Theoretical rejections were calculated based on these values and plotted in Figs. 2 and 3 regarding conductivity and COD, respectively, and the effect of neglecting or not neglecting the CP phenomenon was studied at different concentrations (VCRs). A comparison between model predictions and experimental results was also included.

No experimental points were obtained at low permeate fluxes due to the physical limitations of the RO rig when working at the conditions tested, but several authors have demonstrated the model compliance in this part of the curve for experiments at laboratory scale [36,37]. However, in spite of the fact that both models predict very low rejections at low permeate flux regardless of the feed concentration, the theoretical rejections, specifically those of COD, are very high even for low solute concentrations at low permeate fluxes. This could be considered as a limitation of the models and generate a point of controversy [15]. What is more, there are some examples in the literature where the rejection predicted by the models did not converge towards zero at low permeate flux [35,38].

When neglecting CP (Figs. 2(a) and 3(a)), the SK model predicted the whole range of conductivity rejections and those of COD at low pressures well, but failed to predict the COD rejection values at permeate fluxes higher than approximately 80 L/hm^2, which corresponds to a value of ΔP exceeding 15 bar. The existence of this critical pressure has been previously observed in other NF and RO applications [39]. Above

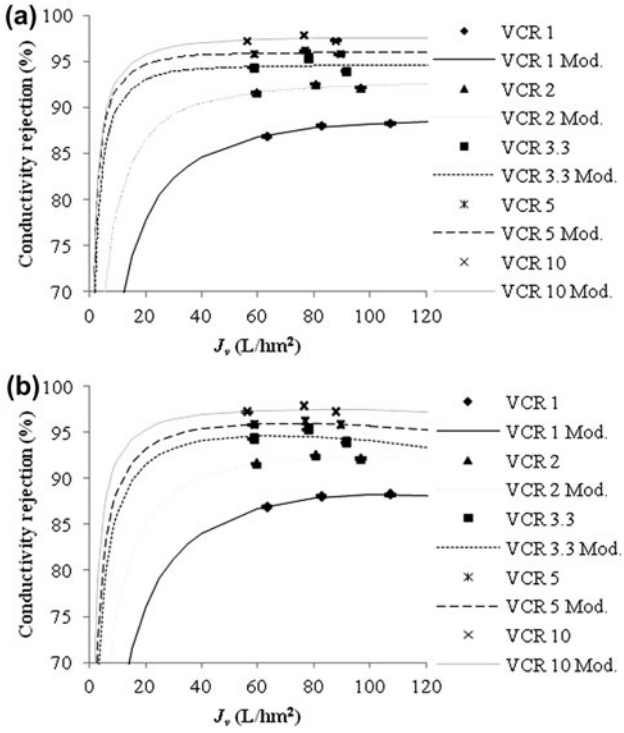

Fig. 2. Experimental and theoretical conductivity rejections vs. permeate flux (J_v) at different volume concentration ratios (VCRs) when considering the Spiegler–Kedem (SK) model (a) or the combined–film theory–Spiegler–Kedem (CFSK) model (b) (symbols: experimental rejections; lines: model predictions).

Table 2
Model parameter estimation when neglecting concentration polarisation (CP) (Spiegler–Kedem (SK) model) and when considering CP (combined–film theory–Spiegler–Kedem (CFSK) model)

			SK model		CFSK model		
	VCR	Concentration	P_s, L/hm^2	σ, %	P_s, L/hm^2	σ, %	k, L/hm^2
Conductivity, μS/cm	1	197.5 ± 10.6	3.810	88.79	5.209	99.97	106.474
	2	335.0 ± 22.1	2.046	92.59	2.819	99.99	92.253
	3.3	499.3 ± 55.9	0.743	94.55	1.359	99.89	67.291
	5	681.3 ± 63.1	0.583	95.95	1.096	99.96	71.997
	10	1143.0 ± 79.0	0.597	97.61	0.759	99.98	81.541
COD, mgO_2/L	1	67 ± 10	0.373	94.07	0.050	99.98	17.167
	2	105 ± 12	0.239	95.12	0.146	99.91	23.651
	3.3	147 ± 36	0.287	95.62	0.083	99.92	20.536
	5	177 ± 36	0.193	95.90	0.073	99.78	23.566
	10	289 ± 76	0.131	97.87	0.167	99.52	40.875

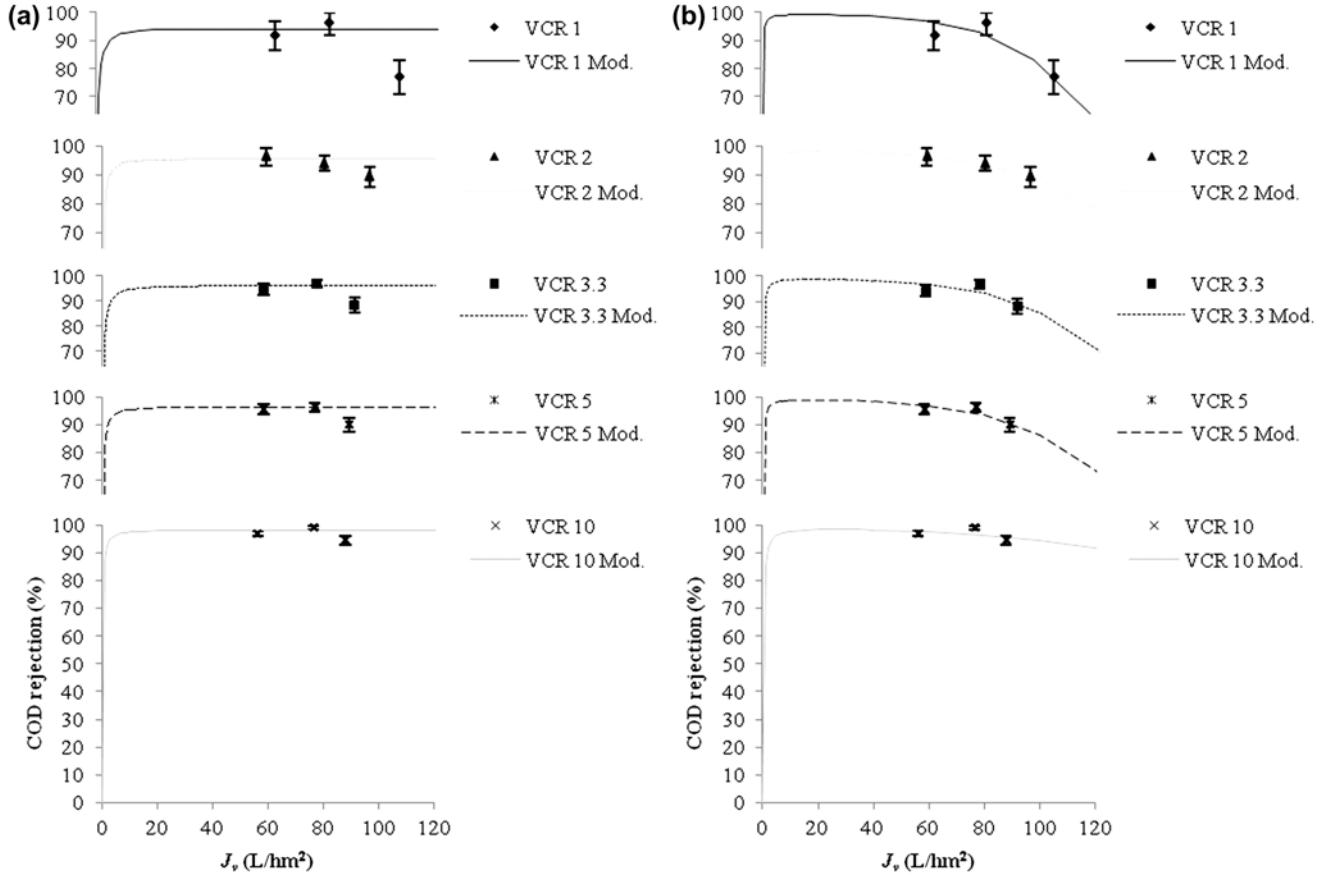

Fig. 3. Experimental and theoretical chemical oxygen demand (COD) rejections vs. permeate flux (J_v) at different volume concentration ratios (VCRs) when considering the Spiegler–Kedem (SK) model (a) or the combined–film theory–Spiegler–Kedem (CFSK) model (b) (symbols: experimental rejections; lines: model predictions).

a given pressure, the drag forces (convective transport), conditioned by the flux into pores, become important and the solute transfer grows, decreasing its rejection [40,41]; until that pressure, the drag forces can be neglected and rejection increases as the solutes are retained by the surface forces (diffusive transport) which are pressure independent [42]. The SK theory predicts an increase in solute rejection (up to an asymptotic value) with flux until the drag forces become dominant [43], but it is unable to predict this maximum rejection observed.

The σ values (expressed in %) of the SK model (Table 2) ranged from 88.79 to 97.61% and from 94.07 to 97.87% regarding conductivity and COD, respectively, and showed very little concentration dependence. The P_s values varied between 0.16×10^{-6} and 1.06×10^{-6} m/s, and between 0.04×10^{-6} and 0.10×10^{-6} m/s for conductivity and COD, respectively. The conductivity P_s values were in the order of those determined by Chaabane et al. [21] (0.35×10^{-6}–2.94×10^{-6} m/s) when studying $Ca/Cu/Cd(NO_3)_2$ and $ZnCl_2$ salt passage (10–100 mg/L) in NF and Rice et al. [18] (1.58×10^{-6}–2.47×10^{-6} m/s) when modelling KCl transport (5–10 mM at pH 7.0–7.5), but well below the values given by Levenstein et al. [16] (16.16×10^{-6}–27.36×10^{-6} m/s) who also modelled NaCl passage (0.5–2.5%). Considering the organic matter P_s, the values are slightly below those calculated by Wadley et al. [44] (0.87×10^{-6} m/s) when modelling organic rejection by NF. These data are included for reference; however, it is difficult to draw final conclusions by comparing the values obtained by different authors as these parameters are strongly influenced by the conditions used (temperature, pressure range, etc.), the type of solute-solvent-membrane interactions and the membrane material as, for example, a smaller pore size implies a greater contribution of the diffusion mechanism conditioning the P_s value.

In this work, the increase in feed concentration caused a rise in the reflection coefficient and a reduction in the salt permeability, contrary to the trend observed in other studies [16,36]. This opposed effect,

characteristic of charged membranes, was explained by these authors as an increase in the ionic strength with concentration producing a shielding phenomenon which neutralises the membrane charge and decreases the repulsion forces. However, although it may be considered an atypical behaviour, there are certain examples in the literature where the authors also observed an increase in the rejection [45,46] and a reduction in the salt permeability [47] with concentration. Symmetric salts (NaCl, KCl, etc.) usually showed a rejection decrease with concentration, while non-symmetric ones ($MgCl_2$, $CaCl_2$, etc.) tended to behave in the opposite way [48]. However, as the rejection and the salt permeability are conditioned by the specificity of the membrane, the solute species involved and the concentration range, a general behaviour cannot be established [37]. In fact, it should be borne in mind that, due to the low solute concentrations used in this work, the possibility of reaching the concentration from which the rejection starts to decrease has not yet been put in evidence. On the other hand, this modification in the charge density of the membrane may result in swelling of the pores and lead to a reduction in the rejection of neutral organic compounds [49]. Nevertheless, there was neither evidence about that in this work nor in others, like Garcia-Aleman et al. [13], for example, who studied the rejection of lactose in a mixed solute system with NaCl.

The relative contribution of diffusive ($J_{diffusive}$) and convective flux ($J_{convective}$) on solute transport was also calculated using Eq. (8), the main results being shown in Table 3. This calculation methodology was proposed by Gilron et al. [23], being applied in the study of monovalent salt–polyvalent ion mixture passage through NF membranes.

$$J_s = J_{diffusive} + J_{convective} = P_s\left(C_m - C_p\right) + J_v C_{lm}(1-\sigma) \quad (8)$$

where C_{lm} is the log mean average between C_m and C_p. C_m was approximated to a C_f value recalculated by applying the model R_{est}.

According to these data, organic transport proved to be dominated by convection, its contribution being around 80%, a circumstance previously observed by Geens et al. [50], who modelled the organic transport in non-aqueous NF. Kim et al. [51] also obtained similar results when studying the transport of organic species through NF and RO membranes and they stated that convection is dominant in most cases except in the passage of hydrophobic non-polar compounds where the diffusion term can be more important. Moreover, they found that permeability in NF membranes seemed to be dominated more by convection than in RO, as expected. In these cases, the reflection coefficient can be approximated to the solute rejection as the diffusive term hardly contributes to solute transport [22]. Regarding the transport of charged species and in general, the convective term represented at least half of the salt flux, which is in good agreement with the results obtained by Gilron et al. [23]. It could be observed that the convective contribution increased with the pressure applied as expected and was at a minimum at the higher feed concentration (VCR 10) as the concentration gradient gained relevance [41].

Table 3
Contribution of convective flux ($J_{convective}$) to solute transport at different volume concentration ratios (VCRs) and pressures (the diffusive influence is given by the difference)

		$J_{convective}$, %		
	VCR	10 bar	15 bar	20 bar
Conductivity	1	47.70	53.55	59.46
	2	46.31	53.28	57.60
	3.3	59.64	66.21	69.71
	5	55.98	62.50	65.89
	10	38.32	45.36	48.71
COD	1	78.06	82.29	85.78
	2	80.00	84.43	86.70
	3.3	74.00	79.12	81.66
	5	79.54	83.64	85.57
	10	70.36	76.34	78.76

The CFSK model, which considers the concentration polarisation effect, was evaluated (Figs. 2(b) and 3(b) and Table 2). CP increases with pressure and can modify the membrane separation properties leading to a decrease in rejection [40,42]. In this work, the COD rejection was reduced by 4.5–19.9% when ΔP increased from 15 to 20 bar. For this model, the estimated P_s values were in the order of those obtained by the SK model, and the σ values (in %), which were near 100%, could be closer to representing an RO membrane than those calculated using SK. Regarding the study of k values, they were compared in Table 4 with those obtained by the graphical method described by Murthy and Gupta [52] and Wang et al. [53] considering the assumptions of the combined–film theory–solution–diffusion (CFSD) model. This method lies in plotting ln [$(1-R_{obs})$ J_v/R_{obs}] vs. J_v and evaluating the slope of the corresponding straight line, which corresponds with the reciprocal of the mass transfer coefficient (k^{-1}). As can be seen in Table 4, both the data obtained by the

Table 4
Comparison between the mass transfer coefficients (k) obtained by the combined–film theory–Spiegler–Kedem (CFSK) and the combined–film theory–solution–diffusion (CFSD) models

		k (L/hm^2)	
	VCR	CFSK	Graphical CFSD
Conductivity	1	106.474	107.527
	2	92.253	91.743
	3.3	67.291	66.667
	5	71.997	71.429
	10	81.541	80.645
COD	1	17.167	23.697
	2	23.651	23.310
	3.3	20.536	28.818
	5	23.566	24.630
	10	40.875	40.984

CFSK model and those obtained by the CFSD methodology are strongly consistent. The effect of CP seemed to be more significant in the case of organics (lower k values), the performance of this specific application being powerfully controlled by the organic load [31]. Although, as the mass transfer coefficient was defined by D/δ and assuming a polarisation layer only of equivalent thickness, the discrepancy observed in the k values when modelling inorganic and organic matter could be associated with the difference in the diffusivities of the species involved. It should be also noted in Figs. 2(b) and 3(b) that the maximum rejections for the different concentrations (VCRs) were approximately reached when the J_v acquired the same value as the corresponding k, a circumstance previously observed by other researchers [52]. This condition is characteristic of the model; that is to say, if the CFSD model equation is differentiated with respect to J_v and the derivative set to zero, the result is that the J_v which produces the maximum rejection matches with the mass transfer coefficient, and this fact is independent of the membrane transport parameters.

Finally, the precision of both the SK and the CFSK models for predicting the conductivity and COD rejections was checked and compared as shown in Table 5, where the relative error between R_{obs} and the R_{est} was calculated.

When using the SK model, the errors varied in the range of 0.05–0.84% and 0.26–18.09% for the conductivity and COD, respectively. On the other hand, they moved in the range of 0.01–0.79% and 0.16–4.84% for the conductivity and COD, respectively, when applying the CFSK model. No significant differences were found when modelling the conductivity rejection; however, in the case of COD, the average error was

Table 5
Relative errors calculated between the observed rejection (R_{obs}) and predicted rejection (R_{est}) when considering Spiegler–Kedem (SK) or combined–film theory–Spiegler–Kedem (CFSK) modelling

		Conductivity					COD				
VCR	J_v, L/hm^2	R_{obs}, %	R_{est} SK, %	[a]E1, %	R_{est} CFSK, %	[b]E2, %	R_{obs}, %	R_{est} SK, %	E1, %	R_{est} CFSK, %	E2, %
1	63.22	86.89	86.99	0.12	86.99	0.12	91.94	94.07	2.27	96.62	4.84
	82.54	88.07	87.84	0.27	87.92	0.17	96.20	94.07	2.27	92.15	4.40
	107.12	88.21	88.34	0.15	88.23	0.01	77.05	94.07	18.09	77.79	0.96
2	59.27	91.59	91.69	0.11	91.70	0.12	96.23	95.12	1.16	96.53	0.31
	80.34	92.52	92.20	0.34	92.26	0.28	94.02	95.12	1.16	93.57	0.47
	96.58	92.16	92.38	0.23	92.31	0.16	89.25	95.12	6.18	89.39	0.16
3.3	58.39	94.32	94.48	0.17	94.63	0.33	94.48	95.62	1.19	96.91	2.50
	77.71	95.33	94.54	0.84	94.58	0.79	96.76	95.62	1.19	93.74	3.22
	91.31	93.92	94.55	0.66	94.34	0.44	88.39	95.62	7.56	89.55	1.29
5	58.39	95.84	95.88	0.05	95.91	0.08	95.65	95.90	0.26	96.97	1.36
	76.83	96.15	95.93	0.23	95.97	0.19	96.15	95.90	0.26	94.11	2.18
	89.13	95.77	95.94	0.19	95.87	0.11	89.86	95.90	6.31	90.75	0.98
10	56.20	97.24	97.33	0.09	97.36	0.12	96.83	97.87	1.06	97.68	0.87
	76.39	97.84	97.49	0.35	97.50	0.34	98.91	97.87	1.06	96.61	2.38
	87.81	97.28	97.54	0.26	97.49	0.22	94.44	97.87	3.50	95.71	1.32

[a]E1: relative error associated with the SK model.
[b]E2: relative error associated with the CFSK model.

decreased (from 3.57 to 1.82%), as well as the maximum error (from 18.09 to 4.84%), when checking the SK results against those of the CFSK model, which reveals the predictive advantages offered by the latter. In the case of COD, it should be noticed that the error estimated when applying the CFSK model was highly improved at high pressure regarding those values calculated for the SK model.

4. Conclusions

Unlike synthetic solutions, industrial streams, as they are the UHT condensates from a commercial dairy, involve complex multi-component mixtures which usually undergo a strong fluctuation in their composition, a circumstance that adds extra complexity in the prediction of the membrane performance when modelling. This heterogeneity made the different inorganic and organic species to be encompassed and measured in terms of conductivity and COD, respectively. The feed stream, which can be considered as low polluted, showed characteristics in the range of 197.5 ± 10.6–1143.0 ± 79.0 μS/cm for conductivity and 67 ± 10–289 ± 76 mgO_2/L for COD, when working at increasing VCR (1–10).

The SK and CFSK models were brought face to face to evaluate their rejection predictions with the permeate flux at different simulated feed concentrations when reversible fouling phenomena could be present. The SK model failed to predict those COD rejections at permeate fluxes higher than 80 L/hm^2, in other words, those values reached when exceeding 15 bar of pressure. The P_s and σ values (expressed in %) varied in the range of 0.16×10^{-6}–1.06×10^{-6} m/s and 0.04×10^{-6}–0.10×10^{-6} m/s, and 88.79–97.61% and 94.07–97.87% regarding conductivity and COD, respectively; these parameters being in the order of those found in the literature. On the other hand, the solute transport was shown to be dominated (≈80%) by convection when modelling COD rejection, but the diffusion term acquired relevance in the case of conductivity (≈50%).

The consideration of concentration polarisation by the film theory explained the maximum rejection observed regarding COD. As a result, the relative error between the observed and predicted rejection was decreased from 3.57 to 1.82% when introducing the mass transfer coefficient as a third fitting parameter. The k values of the CFSK model, which were between 81.5 and 106.5 L/hm^2, and between 17.2 and 40.9 L/hm^2 for conductivity and COD, respectively, were shown to be in good agreement with those calculated by the CFSD graphical methodology.

Nomenclature

Abbreviations

BF	—	bag filter
CFSD	—	combined–film theory–solution–diffusion
CFSK	—	combined–film theory–Spiegler–Kedem
COD	—	chemical oxygen demand
CP	—	concentration polarisation
F	—	prefilter
FC	—	flash cooler
FD	—	flow detector
FI	—	flow meter
HX	—	heat exchanger
NF	—	nanofiltration
P	—	pump
PI	—	pressure indicator
PV	—	pressure vessel
RO	—	reverse osmosis
SDI	—	silt density index
SK	—	Spiegler–Kedem
TFC	—	thin film composite
TI	—	temperature indicator
TK	—	tank
UHT	—	ultra-high temperature
V	—	valve
VCR	—	volume concentration ratio

Symbols

C	—	solute concentration (mg/L or mg/m^3)
C_f	—	feed concentration (mg/L or mg/m^3)
C_{lm}	—	log mean average concentration (mg/L or mg/m^3)
C_m	—	membrane surface concentration (mg/L or mg/m^3)
C_p	—	permeate concentration (mg/L or mg/m^3)
D	—	diffusivity (m^2/s)
dC/dx	—	concentration gradient (mg/Lm or mg/m^4)
E1	—	relative error associated with the SK model (%)
E2	—	relative error associated with the CFSK model (%)
$J_{convective}$	—	convective flux (mg/m^2s or mg/m^2 h)
$J_{diffusive}$	—	diffusive flux (mg/m^2s or mg/m^2 h)
J_s	—	solute flux (mg/m^2s or mg/m^2 h)
J_v	—	permeate flux (m/s or L/hm^2)
k	—	mass transfer coefficient (m/s or L/hm^2)
L_p	—	membrane permeability (m/sbar or L/hm^2 bar)
P_s	—	solute permeability (m/s or L/hm^2)
R_{est}	—	estimated rejection (%)
R_{obs}	—	observed rejection (%)
V_c	—	concentrate volume (m^3 or m^3/h)
V_f	—	feed volume (m^3 or m^3/h)
V_p	—	permeate volume (m^3 or m^3/h)
δ	—	polarisation layer thickness (m)
ΔP	—	transmembrane pressure (bar)
Δx	—	membrane thickness (m)
$\Delta\pi$	—	osmotic pressure (bar)
σ	—	reflection coefficient (decimal or %)

References

[1] C. Bellona, J.E. Drewes, P. Xu, G. Amy, Factors affecting the rejection of organic solutes during NF/RO treatment—A literature review, Water Res. 38 (2004) 2795–2809.

[2] M. Soltanieh, W.N. Gill, Review of reverse osmosis membranes and transport models, Chem. Eng. Commun. 12 (1981) 279–363.

[3] J.G. Wijmans, R.W. Baker, The solution-diffusion model: A review, J. Membr. Sci. 107 (1995) 1–21.

[4] A.L. Ahmad, M.F. Chong, S. Bhatia, Mathematical modeling and simulation of the multiple solutes system for nanofiltration process, J. Membr. Sci. 253 (2005) 103–115.

[5] L. Malaeb, G.M. Ayoub, Reverse osmosis technology for water treatment: State of the art review, Desalination 267 (2011) 1–8.

[6] W.R. Bowen, J.S. Welfoot, P.M. Williams, Linearized transport model for nanofiltration: Development and assessment, AlChE J. 48 (2002) 760–773.

[7] A.A. Merdaw, A.O. Sharif, G.A.W. Derwish, Water permeability in polymeric membranes, Desalination 260 (2010) 180–192.

[8] K.S. Spiegler, O. Kedem, Thermodynamics of hyperfiltration (reverse osmosis): Criteria for efficient membranes, Desalination 1 (1966) 311–326.

[9] E.A. Mason, H.K. Lonsdale, Statistical-mechanical theory of membrane transport, J. Membr. Sci. 51 (1990) 1–81.

[10] S.S. Sablani, M.F.A. Goosen, R. Al-Belushi, V. Gerardos, Influence of spacer thickness on permeate flux in spiral-wound seawater reverse osmosis systems, Desalination 146 (2002) 225–230.

[11] T. Fujioka, L.D. Nghiem, S.J. Khan, J.A. McDonald, Y. Poussade, J.E. Drewes, Effects of feed solution characteristics on the rejection of N-nitrosamines by reverse osmosis membranes, J. Membr. Sci. 409–410 (2012) 66–74.

[12] V.K. Gupta, S.-T. Hwang, W.B. Krantz, A.R. Greenberg, Characterization of nanofiltration and reverse osmosis membrane performance for aqueous salt solutions using irreversible thermodynamics, Desalination 208 (2007) 1–18.

[13] J. Garcia-Aleman, J. Dickson, A. Mika, Experimental analysis, modeling, and theoretical design of McMaster pore-filled nanofiltration membranes, J. Membr. Sci. 240 (2004) 237–255.

[14] S. Jain, S.K. Gupta, Analysis of modified surface force pore flow model with concentration polarization and comparison with Spiegler-Kedem model in reverse osmosis systems, J. Membr. Sci. 232 (2004) 45–62.

[15] Y. Garba, S. Taha, N. Gondrexon, G. Dorange, Ion transport modelling through nanofiltration membranes, J. Membr. Sci. 160 (1999) 187–200.

[16] R. Levenstein, D. Hasson, R. Semiat, Utilization of the Donnan effect for improving electrolyte separation with nanofiltration membranes, J. Membr. Sci. 116 (1996) 77–92.

[17] B. Van der Bruggen, C. Vandecasteele, Modelling of the retention of uncharged molecules with nanofiltration, Water Res. 36 (2002) 1360–1368.

[18] G. Rice, A.R. Barber, A.J. O'Connor, G.W. Stevens, S.E. Kentish, Rejection of dairy salts by a nanofiltration membrane, Sep. Purif. Technol. 79 (2011) 92–102.

[19] C. Bellona, M. Marts, J.E. Drewes, The effect of organic membrane fouling on the properties and rejection characteristics of nanofiltration membranes, Sep. Purif. Technol. 74 (2010) 44–54.

[20] O. Kedem, A. Katchalsky, Thermodynamic analysis of the permeability of biological membranes to non-electrolytes, Biochim. Biophys. Acta 27 (1958) 229–246.

[21] T. Chaabane, S. Taha, M. Taleb Ahmed, R. Maachi, G. Dorange, Coupled model of film theory and the Nernst-Planck equation in nanofiltration, Desalination 206 (2007) 424–432.

[22] J. Geens, K. Boussu, C. Vandecasteele, B. Van der Bruggen, Modelling of solute transport in non-aqueous nanofiltration, J. Membr. Sci. 281 (2006) 139–148.

[23] J. Gilron, N. Gara, O. Kedem, Experimental analysis of negative salt rejection in nanofiltration membranes, J. Membr. Sci. 185 (2001) 223–236.

[24] T. Mohammadi, M. Kazemimoghadam, M. Saadabadi, Modeling of membrane fouling and flux decline in reverse osmosis during separation of oil in water emulsions, Desalination 157 (2003) 369–375.

[25] V. Alvarez, S. Alvarez, F.A. Riera, R. Alvarez, Permeate flux prediction in apple juice concentration by reverse osmosis, J. Membr. Sci. 127 (1997) 25–34.

[26] E.M.V. Hoek, J. Allred, T. Knoell, B.-H. Jeong, Modeling the effects of fouling on full-scale reverse osmosis processes, J. Membr. Sci. 314 (2008) 33–49.

[27] S. Shirazi, C.-J. Lin, D. Chen, Inorganic fouling of pressure-driven membrane processes—A critical review, Desalination 250 (2010) 236–248.

[28] A.L. Ahmad, M.F. Chong, S. Bhatia, Mathematical modeling of multiple solutes system for reverse osmosis process in palm oil mill effluent (POME) treatment, Chem. Eng. J. 132 (2007) 183–193.

[29] A. Suárez, T. Fidalgo, M.A. Berdasco, F.A. Riera, UHT condensate recovery by reverse osmosis: A pilot-plant study, Ind. Eng. Chem. Res. 53 (2014) 15237–15244.

[30] A. Suárez, T. Fidalgo, F.A. Riera, Recovery of dairy industry wastewaters by reverse osmosis. Production of boiler water, Sep. Purif. Technol. 133 (2014) 204–211.

[31] A. Suárez, F.A. Riera, Production of high-quality water by reverse osmosis of milk dairy condensates, J. Ind. Eng. Chem. 21 (2015) 1340–1349.

[32] F.A. Riera, A. Suárez, C. Muro, Nanofiltration of UHT flash cooler condensates from a dairy factory: Characterisation and water reuse potential, Desalination 309 (2013) 52–63.

[33] M. Turan, Influence of filtration conditions on the performance of nanofiltration and reverse osmosis membranes in dairy wastewater treatment, Desalination 170 (2004) 83–90.

[34] B. Wendler, B. Goers, G. Wozny, Regeneration of process water containing surfactants by nanofiltration-investigation and modelling of mass transport, Water Sci. Technol. 46 (2002) 287–292.

[35] H.C. van der Horst, J.M.K. Timmer, T. Robbertsen, J. Leenders, Use of nanofiltration for concentration and demineralization in the dairy industry: Model for mass transport, J. Membr. Sci. 104 (1995) 205–218.

[36] L. Suárez, M.A. Diez, R. García, F.A. Riera, Recovery of Na4EDTA from aqueous solutions using nanofiltration, Sep. Purif. Technol. 118 (2013) 144–150.
[37] D. Van Gauwbergen, J. Baeyens, Modelling reverse osmosis by irreversible thermodynamics, Sep. Purif. Technol. 13 (1998) 117–128.
[38] M. Nyström, L. Kaipia, S. Luque, Fouling and retention of nanofiltration membranes, J. Membr. Sci. 98 (1995) 249–262.
[39] B. Cancino-Madariaga, C.F. Hurtado, R. Ruby, Effect of pressure and pH in ammonium retention for nanofiltration and reverse osmosis membranes to be used in recirculation aquaculture systems (RAS), Aquacult. Eng. 45 (2011) 103–108.
[40] L. Paugam, S. Taha, G. Dorange, P. Jaouen, F. Quéméneur, Mechanism of nitrate ions transfer in nanofiltration depending on pressure, pH, concentration and medium composition, J. Membr. Sci. 231 (2004) 37–46.
[41] P.-Y. Pontalier, A. Ismail, M. Ghoul, Mechanisms for the selective rejection of solutes in nanofiltration membranes, Sep. Purif. Technol. 12 (1997) 175–181.
[42] A. Sorin, A. Favre-Réguillon, S. Pellet-Rostaing, M. Sbaï, A. Szymczyk, P. Fievet, M. Lemaire, Rejection of Gd(III) by nanofiltration assisted by complexation on charged organic membrane: Influences of pH, pressure, flux, ionic strength and temperature, J. Membr. Sci. 267 (2005) 41–49.
[43] A. Dobrak, B. Verrecht, H. Van den Dungen, A. Buekenhoudt, I.F.J. Vankelecom, B. Van der Bruggen, Solvent flux behavior and rejection characteristics of hydrophilic and hydrophobic mesoporous and microporous TiO_2 and ZrO_2 membranes, J. Membr. Sci. 346 (2010) 344–352.
[44] S. Wadley, C.J. Brouckaert, L.A.D. Baddock, C.A. Buckley, Modelling of nanofiltration applied to the recovery of salt from waste brine at a sugar decolourisation plant, J. Membr. Sci. 102 (1995) 163–175.
[45] C. Labbez, P. Fievet, A. Szymczyk, A. Vidonne, A. Foissy, J. Pagetti, Retention of mineral salts by a polyamide nanofiltration membrane, Sep. Purif. Technol. 30 (2003) 47–55.
[46] T. Van Gestel, C. Vandecasteele, A. Buekenhoudt, C. Dotremont, J. Luyten, R. Leysen, B. Van der Bruggen, G. Maes, Salt retention in nanofiltration with multilayer ceramic TiO_2 membranes, J. Membr. Sci. 209 (2002) 379–389.
[47] P. Lipp, R. Gimbel, F.H. Frimmel, Parameters influencing the rejection properties of FT30 membranes, J. Membr. Sci. 95 (1994) 185–197.
[48] C. Mazzoni, S. Bandini, On nanofiltration Desal-5 DK performances with calcium chloride–water solutions, Sep. Purif. Technol. 52 (2006) 232–240.
[49] G. Bargeman, J.M. Vollenbroek, J. Straatsma, C.G.P.H. Schroën, R.M. Boom, Nanofiltration of multi-component feeds. Interactions between neutral and charged components and their effect on retention, J. Membr. Sci. 247 (2005) 11–20.
[50] J. Geens, A. Hillen, B. Bettens, B. Van der Bruggen, C. Vandecasteele, Solute transport in non-aqueous nanofiltration: Effect of membrane material, J. Chem. Technol. Biotechnol. 80 (2005) 1371–1377.
[51] T.-U. Kim, J.E. Drewes, R. Scott Summers, G.L. Amy, Solute transport model for trace organic neutral and charged compounds through nanofiltration and reverse osmosis membranes, Water Res. 41 (2007) 3977–3988.
[52] Z.V.P. Murthy, S.K. Gupta, Sodium cyanide separation and parameter estimation for reverse osmosis thin film composite polyamide membrane, J. Membr. Sci. 154 (1999) 89–103.
[53] R. Wang, Y. Li, J. Wang, G. You, C. Cai, B.H. Chen, Modeling the permeate flux and rejection of nanofiltration membrane separation with high concentration uncharged aqueous solutions, Desalination 299 (2012) 44–49.